

On Zonal Jets in Oceans

Balasubramanya T. Nadiga

Los Alamos National Laboratory, MS-B296, Los Alamos, NM-87545

arXiv:0712.0857v1 [physics.flu-dyn] 6 Dec 2007

Balasubramanya T. Nadiga, MS-B296, Los Alamos, NM-87545; balu@lanl.gov

We find that in parameter regimes relevant to the recently observed alternating zonal jets in oceans, the formation of these jets can be explained as due to an arrest of the turbulent inverse-cascade of energy by *free* Rossby waves (as opposed to Rossby *basin* modes) and a subsequent redirection of that energy into zonal modes. This mechanism, originally studied in the context of alternating jets in Jovian atmospheres and two dimensional turbulence in zonally-periodic configurations survives in spite of the presence of the meridional boundaries in the oceanic context.

1. Introduction

A proposed explanation of the alternating zonal jets in Jovian atmospheres is that they are due to a tendency of turbulence in thin shells on the surface of a rotating sphere to organize itself into zonal jets (e.g., see [Vasavada and Showman, 2005; Galperin et al., 2004]). The anisotropic jets result from an interplay between an inverse cascade of energy [Kraichnan, 1967; Charney, 1947] and the latitudinal variation of the vertical component of planetary rotation (e.g., see [Newell, 1969; Rhines, 1975]). While baroclinic instability and convective processes are thought to be the main sources of small scale energy, classical geostrophic turbulence theory [Charney, 1947] predicts a cascade of this energy (vertically) to larger scales as well in a process that has been termed barotropization. Hence, in the context of this explanation of atmospheric-zonal jets, they have been simulated and studied extensively using the barotropic vorticity equation on either the doubly-periodic or zonally-periodic beta-plane or on the surface of a sphere using forced-dissipative settings. In these settings, the effect of geometry on dynamics is minimized in the sense that the flow in the zonal direction, the direction in which the dynamics of the Rossby waves are highly asymmetric, is homogeneous. Dynamically, the formation of the zonal jets in this homogenous setting is thought to involve certain kinds of resonant interactions (sideband triad and quartet) of Rossby waves packets whose amplitudes are slowly varying functions of space and time [Newell, 1969].

More recently, observational [Maximenko et al., 2005] and computational [Nakano et al., 2005] evidence point to the occurrence of multiple alternating zonal jets in the world oceans as well. However, the dynamics underlying their formation is not clear.

On the one hand, given that the governing equations are the same in the atmospheric and oceanic contexts, it would not be unreasonable to expect, from a turbulence point of view, that the same dynamical mechanism—Rossby wave dispersion arresting the inverse cascade of energy and redirecting it into zonal modes—underlies the phenomenon, be it in the ocean or in the atmosphere. Clearly, unlike the constant stratification of the atmosphere, surface-intensified stratification in the oceans inhibits full barotropization (e.g., see [Fu and Flierl, 1980]). Nevertheless, the importance of the barotropic mode (with a thermocline depth of 1 km in a 5 km deep ocean) is clearly borne out in Fig. 2 and Table 1 of Fu & Flierl [1980] and other such studies confirm an inverse cascade of barotropic kinetic energy. High vertical coherence of jet structure in models [Nakano et al., 2005; Maximenko et al., 2005] further suggests the importance of barotropic dynamics.

On the other hand, the presence of boundaries can, besides being able to support viscous boundary layers and act as sources/sinks of enstrophy, allow for new (inviscid) mechanisms. For example, in a closed basin, (a) Fofonoff gyres arise as statistical equilibrium solutions of the barotropic vorticity equation, and (b) Rossby basin modes arise, resonant interactions of which have been studied as mechanisms for generating both mean flows (starting with Pedlosky [1965]) and mesoscale variability (starting with [Harrison and Robinson [1979]]). Such mechanisms could possibly generate alternating zonal jets as well. Interestingly, LaCasce [2002] finds that the arrest of the inverse cascade of energy by basin normal modes is largely isotropic. However, in a recent article studying rectification processes in a three layer quasi-geostrophic beta plane basin, Berloff [2005] concludes that the alternating zonal jets he found in that setting were most likely driven

by nonlinear interactions between some meridionally structured baroclinic basin modes and some secondary (i.e., related to finite amplitude background flows) basin modes. If this were to be the most important mechanism for the formation of alternating zonal jets in ocean basins, by involving spatially-nonlocal (basin) modes this mechanism would be fundamentally different from the (spatially) local arguments of turbulence that are usually thought to apply in the atmospheric context.

In this letter, we demonstrate that in parameter regimes relevant to alternating zonal jets in the oceans, such jets can be formed by *free* Rossby waves (as opposed to Rossby *basin* modes) arresting the inverse-cascade of energy. We then go on to show that the jet width scales well with Rhines' scale. This suggests that the dynamics of alternating zonal jets in oceans are likely local and in this sense similar to those in previously studied atmospheric contexts. We suggest that the nonlocal resonant-interaction-of-basin-modes mechanism becomes more important at larger values of turbulent kinetic energy (TKE). Curiously, only the latter regime has been investigated before within the framework of the barotropic vorticity equation [LaCasce, 2002], and as far as we know this is the first time that alternating zonal jets have been obtained in a closed basin using the barotropic vorticity equation.

The rest of the letter is structured as follows: The next section briefly describes the modeling approach, and the following one presents computational results. As a matter of convenience, and with no loss of generality, these two sections consider the governing equations and present the results in a nondimensional form. The final section establishes

the correspondence between the nondimensional parameter values considered and their dimensional counterparts in actual ocean settings.

2. Modeling Approach

We consider the barotropic vorticity equation

$$\frac{\partial q}{\partial t} + J(\psi, q) = F + D \quad (2.1)$$

for the evolution of barotropic potential vorticity $q = \zeta + \beta y = \nabla^2 \psi + \beta y$, where ζ is relative vorticity, ψ is velocity streamfunction, F is forcing, D is dissipation and $J(,)$ is the Jacobian operator given by $J(\psi, q) = -\frac{\partial \psi}{\partial y} \frac{\partial q}{\partial x} + \frac{\partial \psi}{\partial x} \frac{\partial q}{\partial y}$. The above equation is considered on a midlatitude beta plane with a latitudinal gradient of the vertical component of rotation of β ; y-coordinate increases northwards and x-coordinate eastwards in a closed square basin, 2π on a side, discretized into 1024×1024 cells. An energy and enstrophy conserving finite-differencing is used with Runge-Kutta timestepping [Greatbatch and Nadiga, 2000]. Given the inverse-cascade of energy of 2D turbulence, forcing F is concentrated around a high wavenumber k_f , as a combination of sines and cosines consistent with the boundary conditions used. Their amplitudes σ , drawn randomly from a Gaussian distribution, are delta-correlated in time resulting in $F = \sigma(t)/\sqrt{\delta t} f(k_f, t)$ with an energy input rate ϵ of $\sigma^2 \iint f \nabla^{-2} f dx dy$ and an enstrophy input rate η of $k_f^2 \epsilon$. In all the computations presented, given the domain size of $2\pi \times 2\pi$ discretized into 1024×1024 cells, k_{max} is 512 and k_f is between 128 and 129.

Dissipation $D = -\nu_p \nabla^{2p} \zeta - \nu_0 \zeta$, consisting of a small-scale-selective component to dissipate the (largely) downscale-cascading enstrophy input at the forcing scale, and Rayleigh friction component that mainly acts to dissipate the (largely) upscale-cascading

energy. At lateral boundaries, besides no through-flow, we use superslip boundary conditions. The coefficient ν_p is diagnosed dynamically in terms of the enstrophy input rate as $\nu_p = C_K \eta^{\frac{1}{3}} \Delta x^{2p}$, using Kolmogorov-like ideas and a Kolmogorov scale of Δx .

Given the above setup, the problem consists of three important parameters: β , ϵ and ν_0 . We briefly recall a few relevant spatial scales in terms of these parameters. First, in purely two-dimensional turbulence, a Kolmogorov scale for the dissipation of energy may be obtained using the usual arguments as

$$k_{fr} = (3C_K)^{\frac{3}{2}} \left(\frac{\nu_0^3}{\epsilon} \right)^{\frac{1}{2}} \approx 50 \left(\frac{\nu_0^3}{\epsilon} \right)^{\frac{1}{2}} \quad (2)$$

(e.g., see [Danilov and Gurarie, 2002]). In the absence of β this would be the scale at which Rayleigh friction would act to stop the inverse cascade of energy. However, in the presence of β , Rossby wave dispersion can instead arrest the inverse cascade and redirect energy into zonal modes. In the absence of large scale friction, and under the assumption that the spectral flux of energy in the inverse-cascade inertial range is determined by the energy input rate ϵ (due to forcing), this would happen at $k_\beta = (\beta^3/\epsilon)^{1/5}$ [Vallis and Maltrud, 1993]. If, however, energy is concentrated near k_β , this arrest mechanism would occur at the Rhines' scale $k_\beta^R = \sqrt{\beta/U_{rms}}$ [Rhines, 1975] (also obtained by equating the turbulence frequency $U|k_\beta|$ and the Rossby wave frequency $-\beta \cos \phi/|k_\beta|$, where $\phi = \tan^{-1} k_y/k_x$). Given the largely upscale-cascading nature of energy, the small-scale-selective dissipation operator plays a relatively minor role in dissipating energy, so that $dE/dt \approx \epsilon - 2\nu_0 E$, with energy leveling off at about $\epsilon/2\nu_0$. Using this energy balance in the expression for Rhines' scale leads to [Danilov and Gurarie, 2002; Smith et al., 2002]

$$k_\beta^R = \left(\frac{\beta}{2} \right)^{\frac{1}{2}} \left(\frac{\nu_0}{\epsilon} \right)^{\frac{1}{4}}. \quad (3)$$

3. Results

Table 1 gives the basic parameters and the derived scales discussed above for a series of simulations. In all the cases considered, care is taken to ensure that the spectrum of the zonal component of energy has equilibrated. While there are important differences between some of the cases in Table 1, we postpone a detailed discussion of these differences to a later article, and go on to examine a representative case—case C presently. An examination of the instantaneous, zonally-averaged, zonal-velocity and relative-vorticity fields plotted as a function of latitude in Fig. 1 suggests alternating zonal jets of a characteristic width. To further verify this, we examine a few other familiar diagnostics. First, Fig. 2 shows the time-mean two-dimensional zonal-velocity field after the flow has reached statistically-stationarity, and the alternating zonal jets are evident in this figure. Note that a) even though the forcing is homogeneous, the jets are more pronounced to the west, b) unlike with observations, time-mean jet signatures are obtained and analysed, and c) the geometry of the jets are not significantly different when the time-varying components are analysed (not shown). Finally, while the meridional gradient of time-averaged potential-vorticity is dominated by β (stable), the instantaneous flow quite frequently violates the barotropic stability criterion $u_{yy} < \beta$. That these alternating zonal jets are related to anisotropization of the inverse cascade of energy of two dimensional turbulence by Rossby wave dispersion is verified by the dumbbell shape near the origin, characteristic of the process (e.g., see [Vallis and Maltrud, 1993]), in the contour plot of the two dimensional spectral density of energy in Fig. 3.

It is not our intent to verify various universal scalings of spectra in this problem, but to use it as a diagnostic to further confirm the nature of the dynamics. To this end, we show in Fig. 4 the range of spectra that we obtain in the parameter range considered. These figures show the 1D energy spectra averaged over an angle of $\pi/6$ around $\phi = 0$ (residual flow) and $\phi = \pi/2$ (zonal flows) [Chekhlov et al., 1996]. Both the residual and zonal spectra have further been compensated for the $k^{-5/3}$ scaling. (A compensation for $\epsilon^{2/3}$ —following Kolmogorov scaling $E(k) = C_k \epsilon^{2/3} k^{-5/3}$ —is avoided since while that would be appropriate for the residual component, it would not be appropriate for a possibly different scaling of the zonal component such as $E_z(k) = C_z \beta^2 k^{-5}$. However, $\epsilon^{2/3}$ compensation has been applied to the residual spectra to establish the value of the Kolmogorov constant C_k). A common and important feature of all the cases is that in the inverse-cascade regime, while at the high-wavenumber end, the zonal and residual spectra scale similarly, at lower wavenumbers the zonal spectra lie above the residual spectra and show steepening before they peak. This behavior is as expected and verified by various investigators in the periodic case relevant to the atmosphere. Furthermore, like in the computations of Danilov and Gurarie [2001], our spectra display significant non-universal behavior. For example, while in cases A and F, the residual spectra clearly verify the classic Kolmogorov scaling $C_k \epsilon^{2/3} k^{-5/3}$ with a Kolmogorov constant C_k of about 6, that is not the case for cases C and J. We note parenthetically that (a) the distribution of spectral energy flux as a function of wavenumber (not shown) bears remarkable resemblance to that derived using Aviso, TOPEX/Poseidon, and ERS-1/2 data [Scott and Wang, 2005], and (b) on using the spectral flux of energy as a function of wavenumber, as opposed to a constant

value, C_k remains close to 6 in the high wavenumber range of the inverse-cascade, but then begins to rise at the lower wavenumbers.

Next, we identify the jet width with the wavenumber at which the (uncompensated) zonal-spectrum peaks, k_p , and verify it by referring to physical-space pictures like in Figs. 1 and 2. This number is recorded for each of the cases in the last column of Table 1. We note, that the wavenumber at which the residual spectrum peaks is close to this wavenumber as well. In Fig. 5, we plot the above measure of jet width (k_p) against the Rhines' scale (k_β^R) and find excellent agreement, like in the periodic (atmospheric) case (e.g., see Vallis and Maltrud [1993] and Danilov and Gurarie [2001]).

4. Discussion

The simulations and analyses presented in the previous section show clearly that there are parameter regimes wherein the dynamics of the alternating zonal jets in a midlatitude ocean basin are not controlled in a fundamental manner by meridional boundaries. That is to say, in these parameter regimes, the dynamics of the jets are governed largely by spatially local interactions, and the arrest of the inverse-cascade is mediated by free Rossby waves as opposed to Rossby basin modes. However, we still need to check if such a parameter regime is of relevance to the oceans in order to establish the importance of this mechanism in the oceans.

The pronounced signature of the observed jets in western regions of ocean basins (Fig. 1 of [Maximenko et al., 2005]) would generally be attributed to the elevated levels of TKE in the separated western boundary current (WBC) regions. However, our simulations use homogeneous forcing but still display similar enhanced jet signatures in the west. This

leads us to suspect that the enhanced signature of the jets in the west is more due to its internal dynamics, rather than due to the elevated levels of TKE in the WBC regions, and that the jets are controlled more by the ambient (lower) levels of *interior* TKE. An approximate range of 25 to 100 cm²/s² is obtained for the latter by examining an altimetry-derived TKE map for the North Atlantic [pers. comm.; Scott, 2006]. Keeping this in mind, first consider case C discussed extensively above: the peak wavenumber k_p is 26 (Table 1); using the observed [Maximenko et al., 2005] dominant wavelength of 280 km. leads to L_{ref} of 1160 km. Then, using a typical midlatitude value of β_{ref} of $2 \cdot 10^{-11} \text{ m}^{-1}\text{s}^{-1}$ and an r.m.s. value of 7.5 cm/s (mid-range) for the domain-averaged *interior* geostrophic velocity anomaly (TKE), leads to a β_{nd} ($=\beta_{ref}L_{ref}^2/U_{ref}$) of 360, corresponding well with 320 used for case C. As for the ranges of parameters considered, $5 \leq k_p \leq 55$ (Table 1); using a range of wavelengths of 500 to 250 km and domain-averaged *interior* TKE level corresponding to $5 \leq U_{rms} \leq 10$ cm/s, gives β_{nd} in the range 30–1900 (c.f. range of 80–1280 in Table 1). In light of this, we suggest that the local mechanism wherein the arrest of the inverse cascade is mediated by free Rossby waves may be important in explaining the formation of alternating zonal jets in the world oceans. Obviously, further work is necessary to *definitively* establish the relevance of this mechanism to the oceans. The author thanks Boris Galperin for discussions and the referees for their criticism.

References

- P.S. Berloff, On rectification of randomly forced flows, J. Mar. Res., 63, 497–527, (2005)
 J.C. Charney, Geostrophic turbulence, J. Atmos. Sci. 28, 1087–1095 (1947)

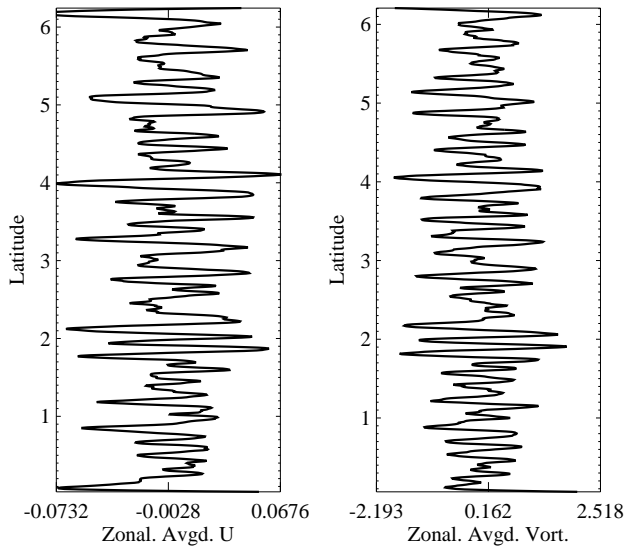
- A. Chekhlov, S.A. Orszag, S. Sukoriansky, B. Galperin (1996) The effect of small-scale forcing on large-scale structures in two-dimensional flows, *Physica D* 98, 321–334
- S. Danilov and D. Gurarie (2001), Nonuniversal features of forced two-dimensional turbulence in the energy range, *Phys. Rev. E* 63, 020203
- S. Danilov and D. Gurarie (2002), Rhines scale and spectra of the β -plane turbulence with bottom drag, *Phys. Rev. E* 65, 067301
- L-L. Fu and G.R. Flierl (1980) Nonlinear energy and enstrophy transfers in a realistically stratified ocean, *Dyn. Atmos. Oceans* 4, 219–246
- B. Galperin et al. (2004), The ubiquitous zonal jets in the atmospheres of giant planets and the Earth's oceans, *Geophys. Res. Lett.*, 31, L13303
- R.J. Greatbatch and B.T. Nadiga (2000), Four gyre circulation in a barotropic model with double gyre wind forcing, *J. Phys. Oceanogr.* 30, 1461–1471
- D.E. Harrison and A.R. Robinson (1979), Boundary-Forced Planetary Waves: A Simple Model Mid-Ocean Response to Strong Current Variability, *J. Phys. Oceanogr.* 9, 919–929
- R.H. Kraichnan (1967), Inertial ranges in two-dimensional turbulence. *Phys. Fluid*, 10, 1417–1423.
- J.H. LaCasce (2002), On turbulence and normal modes in a basin, *J. Mar. Res.* 60, 431–460
- N.A. Maximenko, B. Bang and H. Sasaki (2005), Observational evidence of alternating zonal jets in the world ocean, *Geophys. Res. Lett.* 32, L12607

- H. Nakano and H. Hasumi (2005), A series of zonal jets embedded in the broad zonal flows in the Pacific obtained in eddy-permitting ocean general circulation models, *J. Phys. Oceanogr.* 35, 474–488
- A.C. Newell (1969), Rossby wave packet interactions, *J. Fluid Mech.* 35, 255–271
- J. Pedlosky (1965), A Study of the Time Dependent Ocean Circulation, *J. Atmos. Sci.* 22, 267–272
- P.B. Rhines, Waves and turbulence on a beta-plane, *J. Fluid Mech.*, 69, 417–443, (1975)
- R.B. Scott and F. Wang (2005), Direct Evidence of an Oceanic Inverse Kinetic Energy Cascade from Satellite Altimetry, *J. Phys. Oceanogr.* 35, 1650–1666
- K.S. Smith, G. Boccaletti, C.C. Henning, I. Marinov, C.Y. Tam, I.M. Held, and G.K. Vallis (2002), Turbulent diffusion in the geostrophic inverse cascade, *J. Fluid Mech.* 469, 13–48
- A.R. Vasavada and A.P. Showman (2005), Jovian atmospheric dynamics: an update after Galileo and Cassini, *Rep. Prog. Phys.* 68 (2005) 1935–1996
- G.K. Vallis and M.E. Maltrud (1993), Generation of mean flows and jets on a beta plane and over topography, *J. Fluid Mech.* 228, 321–342

Table 1. Basic parameters, derived scales and the jet-width wavenumber for the ten simulations

considered

Case	β	ϵ	ν_0	k_β	k_{fr}	k_β^R	k_p
A	80	0.50	0.1	15.9	2.2	15.9	17.5
B	160	0.50	0.1	24.1	2.2	22.2	15.5
C	320	0.50	0.1	36.6	2.2	31.3	26
D	640	0.50	0.1	55.5	2.2	38.5	37
E	1280	0.50	0.1	84.0	2.2	66.7	55
F	80	33.5	0.1	6.0	0.2	5.96	4.5
G	80	128	0.4	4.6	0.8	5.88	7
H	1280	126	0.4	27.8	1.1	22.2	20
I	1280	296	0.4	23.4	0.7	18.2	16
J	1280	513	0.4	21.0	0.6	15.9	13

**Figure 1.** Meridional plot of the instantaneous zonally-averaged zonal-velocity and vorticity.

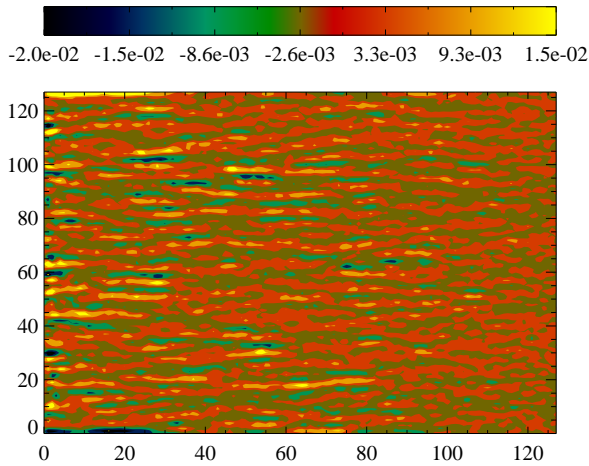


Figure 2. The alternating zonal jets are evident in the time-averaged, two-dimensional zonal-velocity field. While forcing is homogeneous, jets are more prominent in western regions.

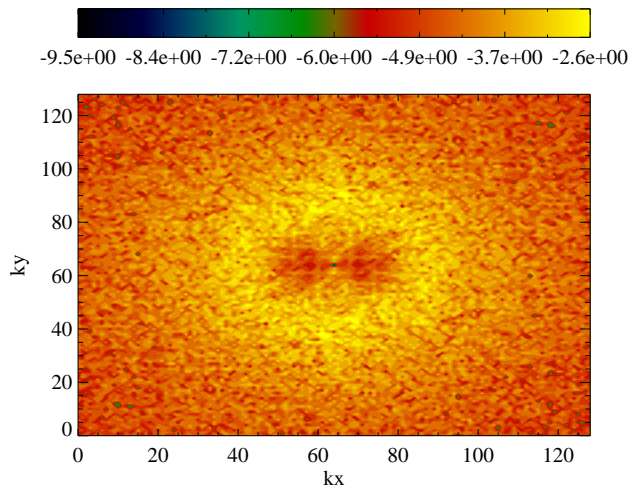


Figure 3. The time-averaged two-dimensional energy spectrum displays the familiar anisotropic 'dumbbell' shape.

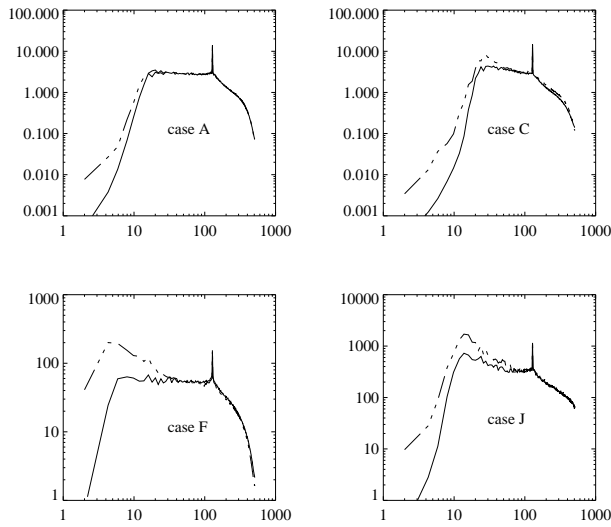


Figure 4. Time-averaged one-dimensional zonal (dot-dashed line) and residual (solid line) energy spectra. Both have a $k^{-5/3}$ compensation. See text for details.

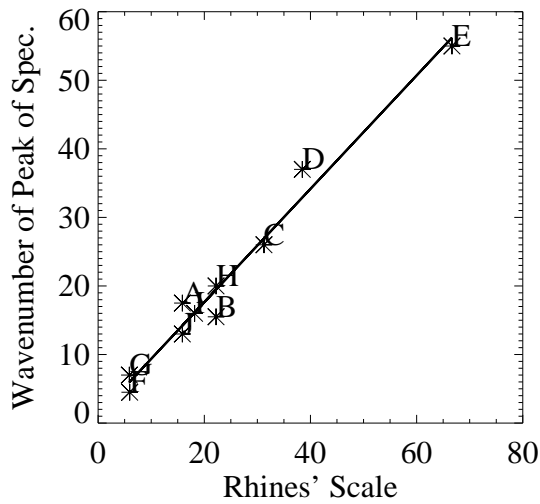


Figure 5. A plot of the wavenumber at which the zonal-spectrum peaks, k_p against the Rhines' scale k_β^R . Symbols correspond to the cases in Table 1 and line to the linear least squares fit.